Heritage Science

RESEARCH

Open Access

Effects of superplasticizer on properties of calcined ginger nuts-based grouting material for earthen site cracks

Xin Wen[1], Nan Wang[2,3], Jingke Zhang[2,3*], Lixiang Zhang[2,3], Yanfei Wei[1] and Wenting Gu[1]

Abstract

Grout injection is an effective technique for repairing cracks in earthen sites. This study aims to address the challenges of Calcined Ginger Nuts (CGN)-based grout and enhance its engineering performance by investigating the compatibility of different superplasticizers. We examined the effects of Polycarboxylate Superplasticizer (PCE) and Naphthalene Superplasticizer (PNS) on the properties of CGN-based grout, focusing on fluidity, rheological properties, mechanical strength, volume stability, color difference, and pore structure. The engineering applicability of the optimized CGN-based grout with superplasticizers was assessed using COMSOL Multiphysics. The results show that fluidity increased with higher dosages of PCE and PNS. The grout containing these superplasticizers behaved as a shear-thinning fluid, following the power law model. Specifically, the consistency coefficient of grout with 0.5 wt% PCE and PNS decreased by 39.73% and 64.83%, respectively. Additionally, 2.9 wt% PCE and PNS reduced volume shrinkage rate by 6.86% and 6.27%, respectively. Initially, increasing the dosage of PCE and PNS improved compressive and flexural strength, but these properties later declined. XRD analysis revealed that PNS above 1.1 wt% and PCE weakened the hydration reaction, while both superplasticizers promoted carbonation. Mercury Intrusion Porosimetry (MIP) showed that 1.1 wt% PCE and PNS reduced the proportion of capillary pores by 13.79% and 10.11%, respectively. Based on these findings, 0.5 wt% PNS demonstrated the best compatibility with CGN-based grout, whereas PCE showed poor compatibility. Numerical simulations using COMSOL Multiphysics confirmed that 0.5 wt% PNS provided superior grouting effectiveness. Therefore, the CGN based grout with 0.5wt% PNS demonstrates excellent engineering performance and applicability. This study offers valuable insights into optimizing CGN-based grout for the preservation of earthen sites.

Keywords Earthen site, Calcined Ginger Nuts, Grouting material, Superplasticizer, Workability, Numerical simulation

Introduction

Earthen sites, such as the Great Wall, the Dadiwan sites, the ancient city of Jiaohe, and the Western Xia mausoleum, are significant cultural relics made primarily of earth. These sites have been central to human activities in production, culture, religion, and war, bearing witness to the historical integration, innovation, prosperity, and development of societies [1]. As such, they hold immense historical, artistic, scientific, and social significance. In fact, over one-third of the cultural heritage sites on the UNESCO World Cultural Heritage list are earthen sites [2].

*Correspondence:
Jingke Zhang
zhangjink@lzu.edu.cn
[1] Gansu Provincial Institute of Cultural Relics and Archaeology, Lanzhou 730000, China
[2] School of Civil Engineering and Mechanics, Lanzhou University, Lanzhou 730000, China
[3] Key Laboratory of Mechanics On Disaster and Environment in Western China With the Ministry of Education, Lanzhou University, Lanzhou 730000, China

Nevertheless, these earthen sites are suffering from various types of deterioration, including cracks, collapses, sapping, erosion, and weathering due to prolonged exposure to natural elements and human activities [3]. Cracks, in particular, pose a significant threat as they compromise the stability and integrity of the structures, allowing water infiltration and accelerating degradation [4]. For instance, many sections of the Beacon Tower and the Great Wall in the northwest of China have been severely affected by cracks [5]. Therefore, addressing crack reinforcement is critical for the preservation of earthen sites.

Through systematic exploration and practical application, the grout injection has become an effective method for reinforcing cracks in earthen sites [6, 7]. Grout play a crucial role in the grouting injection, with their properties impacting the effectiveness of reinforcement extremely. Various binders, such as high mole ratio potassium silicate (PS) [8], polyvinyl alcohol (SH) [9], Natural Hydraulic Lime (NHL) [10], and Calcined Ginger Nuts (CGN) [11], have been developed for this purpose. Among these binders, the CGN has been gained widely attention due to its excellent compatible with earthen sites. Additionally, the grout were enriched with earthen site' s soil derived from the nearly region to ensure congruity with the per-reinforcing materials. Zhang et al. [5, 12] tested the durability of CGN based grout under the indoor and realistic curing condition. Chen et al. [13, 14, 15] proved the compatibility of CGN based grout from the aspect of mechanical properties, hydration properties, and physical properties. The CGN based grout has been recognized as an excellent grout injection material for earthen sites and gradually applied in the reinforcement of earthen sites [16–18].

Previous studies have shown the durability and compatibility of CGN-based grout under different conditions. However, the currently applying CGN based grout face certain challenges in balancing high flowability and low volume shrinkage due to the high specific surface area, water absorption, and flocculation of fine soil particles [19]. To effectively fill cracks and prevent separation from the earthen site, the grout must have adequate fluidity and low volume shrinkage [20].

Simple binder and water formulations of CGN based grout are are insufficient to meet these requirements, a compatible admixture-material particle system is necessary for optimal performance [21]. Superplasticizer have been shown to significantly improve the fluidity of cement-based grout at a constant water-to-cement ratio. The fluidity of cement mortars with PCE and NSF are related to the coverage of the first adsorbed layer [22]. Zhang et al. [24] reported that polycarboxylate ether superplasticizer could effectively reduce yield stress of concrete mortars. Moreover, Chandra S et al. [23] found that different types of superplasticizer would reduce the overall drying shrinkage of cement based grout. Kohandelnia et al. [21, 25] analyzed the effect of various superplasticizer type on the fresh and hardened properties of self-consolidating earth paste (SCEP), this paste is similar with CGN based grout at a larger extent, both belongs to earthen based paste. The rheological and thixotropic properties of various SCEC mixtures proportioned with superplasticizer were also analyzed, and concluded empirical models of predicting rheology of SCEC paste [26]. In addition, NHL is a traditional lime-based binder similar to CGN, Baltazar et al. [27] found that PCE could improve the fluidity and drying shrinkage of NHL grout. Jorne et al. [28] found polycarboxylate ether could reduce the yield stress and plastic viscosity of NHL grouts and thus improving the injectability and injectability rate. Zhu et al. [29] reported that PCE can delay the early hydration of C_2S and the crystallization time of $Ca(OH)_2$, and this retardation effect is inversely proportional to the rheological properties of NHL2 paste. Facing these advantages of superplasticizers on the cement pastes, SCEC mixtures and NHL based pastes, it is of practical significance to study the effects of superplasticizers on fresh and hardened properties of CGN based grout systematically.

Herein, to address existing challenges of CGN-based grout and further improve the engineering performance, this study explores the compatibility of Polycarboxylate Superplasticizer (PCE) and Naphthalene Superplasticizer (PNS). We systematically investigate the effects of different dosages of PCE, PNS on the fluidity and rheological properties of CGN-based suspensions. Additionally, we examine their impact on the mechanical strength, volume shrinkage, color difference, X-ray diffraction (XRD) patterns, and pore structure of CGN-based concretion. Based on these findings, we identify the most compatible superplasticizer for the CGN-based particle system. This optimized superplasticizer-CGN-based grout is then simulated and verified using COMSOL Multiphysics. The outcomes of this research will contribute to the development of more effective grouting materials, supporting the conservation of valuable earthen sites.

Material and experimental methods

Materials

CGN was procured from the material laboratory of Dunhuang Academy, China, while the soil from earthen sites was obtained from the collapsed section of the Great Wall in Gulang County, Gansu Province, China. The mineralogical phases and contents of CGN and earthen site soil were analyzed using X-ray diffractometer (XRD, Rigaku, UltimaIV), with the results presented in Table 1, Table 2. The primary mineral phases of CGN include

Table 1 XRD Semi-quantitative mineral content of CGN

Mineral content (wt%)	CaO	β-$CaSiO_3$	$Ca_2Al_2Si_2O_8$	SiO_2	$Ca(OH)_2$
CGN	31.8	30.6	15.1	18.9	3.5

CaO, β-$CaSiO_3$, and $Ca_2Al_2Si_2O_8$, whereas the main mineral phases of earthen site' soil comprise quartz and plagioclase.

Particle size distribution analyses of CGN and earthen site' soil were conducted using an ultra-high speed intelligent particle size analyzer (Mastersizer 3000, Malvern Panalytical Ltd., UK), with the outcomes depicted in Fig. 1a, b. SEM images of CGN and earthen site' soil were captured using a JSM7200F scanning electron microscope with an UltraDry EDS Detector (JEOL Company, Japan), with the images presented in Fig. 1c, d.

Table 3 Characteristic of superplasticizer

Characteristics of superplasticizer	Polycarboxylate (PCE)	Naphthalene (PNS)
Colour	Colourless liquid	Brown powder
Density (g/cm^3)	1.05–1.10	1.155–0.195
PH	6.0	8.3
Solid content (%)	20.7	100

Two commonly superplasticizers, including Polycarboxylate (PCE), Naphthalene (PNS) were acquired from a construction material market in China, whose basic characteristics are presented in Table 3.

Table 2 XRD Semi-quantitative mineral content of earthen site' soil

Mineral content (wt%)	Quartz	Plagioclase	Orthoclase	Calcite	Anhydrite	Dolomite
Earthen site' soil	51.3	26.6	11.3	5.8	3	2.1

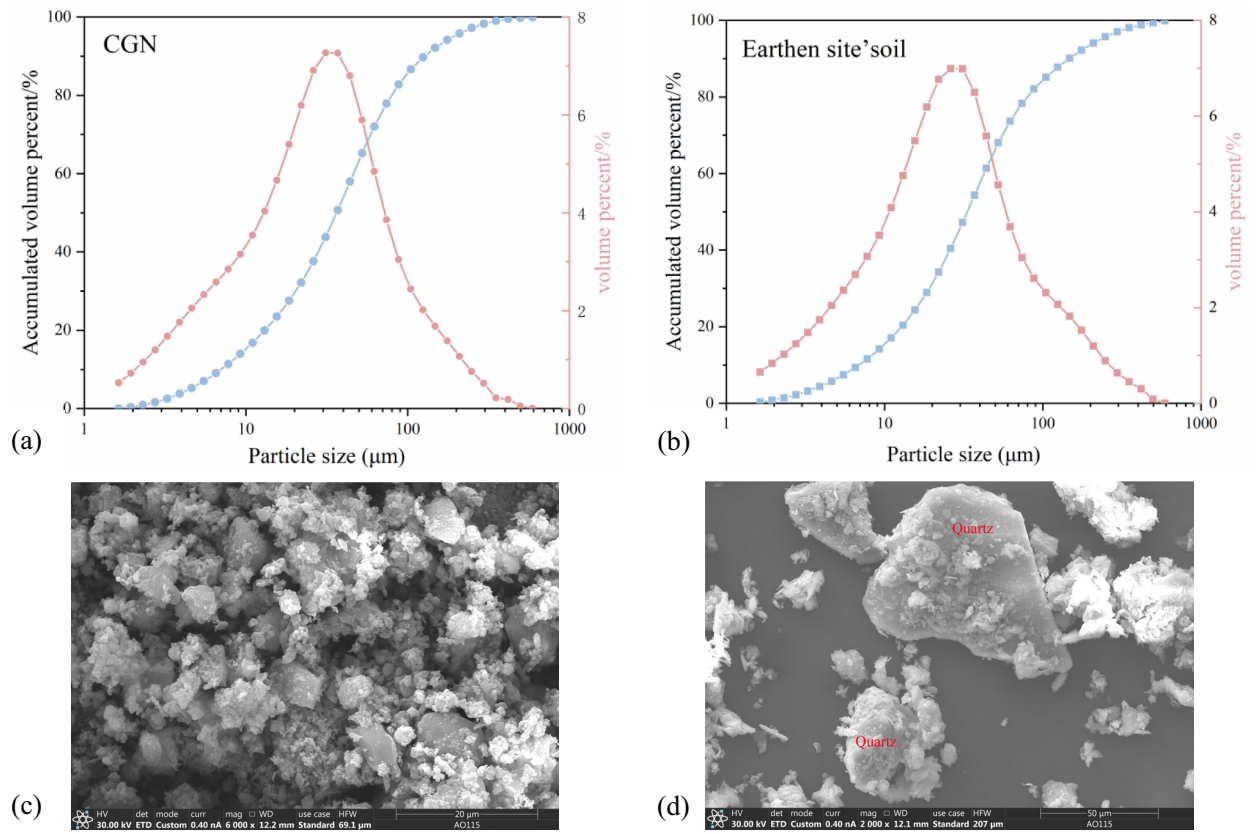

Fig.1 **a** Particle size distribution of CGN, **b** Particle size distribution of earthen site' soil, **c** SEM images of CGN, **d** SEM images of earthen site' soil

Fourier transform infrared spectra of PCE and PNS were conducted using a Spectrum FTIR spectrometer (Nicolet NEXUS 670, USA) in the range from 4000 cm^{-1} to 400 cm^{-1}, with 64 scans per sample at a resolution of 4 cm^{-1}. Based on the FTIR results of PCE (Fig. 2a), broad absorption bands were observed at 3406 cm^{-1}, attributed to O–H, and at 2880 cm^{-1}, attributed to C–H stretching vibrations (–CH_2, –CH_3). The C=O carbonyl group and C–O–C stretching vibration were recorded at 1729 cm^{-1} and 1113 cm^{-1}, respectively. The C–O=O carbonyl group was observed at 525 cm^{-1}. As depicted in Fig. 2b, the main functional groups of PNS include CH_2 and S=O [30].

Grout design

This study maintained consistent water-to-cement (W/C) and binder-to-aggregate ratios to focus on the influence of superplasticizer types and dosages on CGN-based grout characteristics. CGN acted as the binder, complemented by soil from earthen site as the aggregate, with a selected binder-to-aggregate ratio of 1:10 based on prior research [15]. The W/C ratio of 0.46 was chosen following preliminary experiments. PCE and PNS were incorporated at varying concentrations (0.5 wt%, 1.1 wt%, 1.7 wt%, 2.3 wt%, and 2.9 wt% of the total CGN and soil weight), guided by initial tests. Each mix group included three parallel specimens to ensure reliability. Detailed mix proportions are provided in Table 4, facilitating a systematic evaluation of the effects of PCE, PNS on CGN-based grout properties.

Superplasticizers can be incorporated into geopolymer mixes through different methods, such as adding them as raw materials or including them in the mixing solution [31]. Yan et al. [32] concluded that adding superplasticizer as a raw material powder yielded better results. Consequently, in subsequent experiments, superplasticizer was initially introduced as a raw material powder for pre-mixing. The production stages of the grout are described below [33]. The experimental procedure is illustrated schematically in Fig. 3.

Table 4 Mix proportions of CGN-based grout

Samples	PCE/PNS dosage	Binder-to-aggregate ratio	W/C ratio	Parallel specimens number
Control group	0	1:10	0.46	3
0.5% PCE/PNS	0.5wt%	1:10	0.46	3
1.1% PCE/PNS	1.1wt%	1:10	0.46	3
1.7% PCE/PNS	1.7wt%	1:10	0.46	3
2.3% PCE/PNS	2.3wt%	1:10	0.46	3
2.9% PCE/PNS	2.9wt%	1:10	0.46	3

- Firstly, Calcined Ginger Nuts (CGN) and earthen site' soil were meticulously mixed with a trowel for 3 min to ensure homogeneous blending of the materials.
- Subsequently, water and either PCE or PNS were simultaneously added within 30 s, while an electric mixer continued stirring for an additional 30 s. The mixing process was maintained for 3 min at a speed of 285 ± 10 r/min.
- Following mixing, the homogeneous mixture was poured into steel molds measuring 40 mm × 40 mm × 160 mm and vibrated on a vibrat-

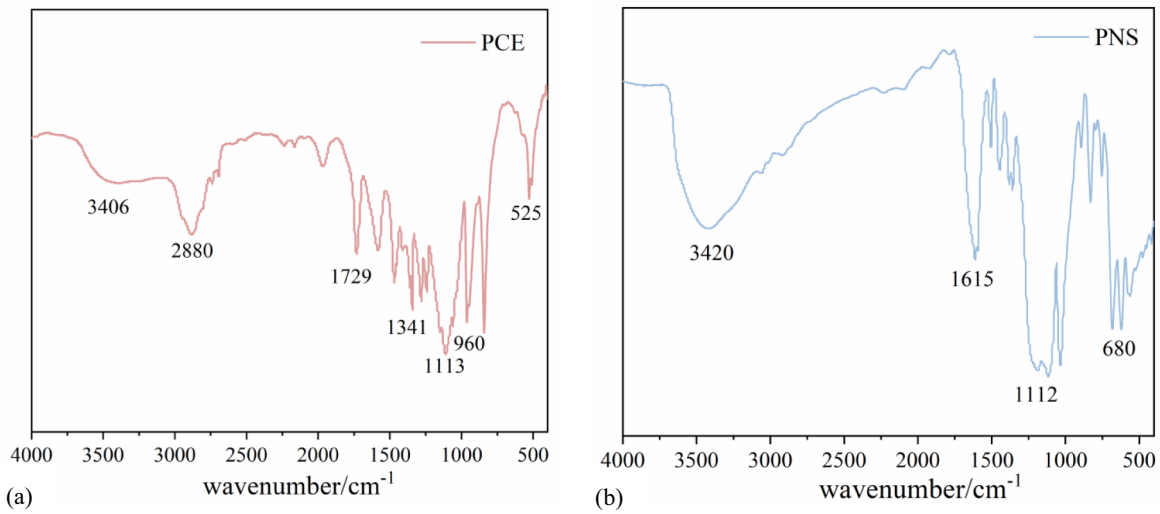

Fig. 2 **a** The FTIR pattern of PCE, **b** The FTIR pattern of PNS

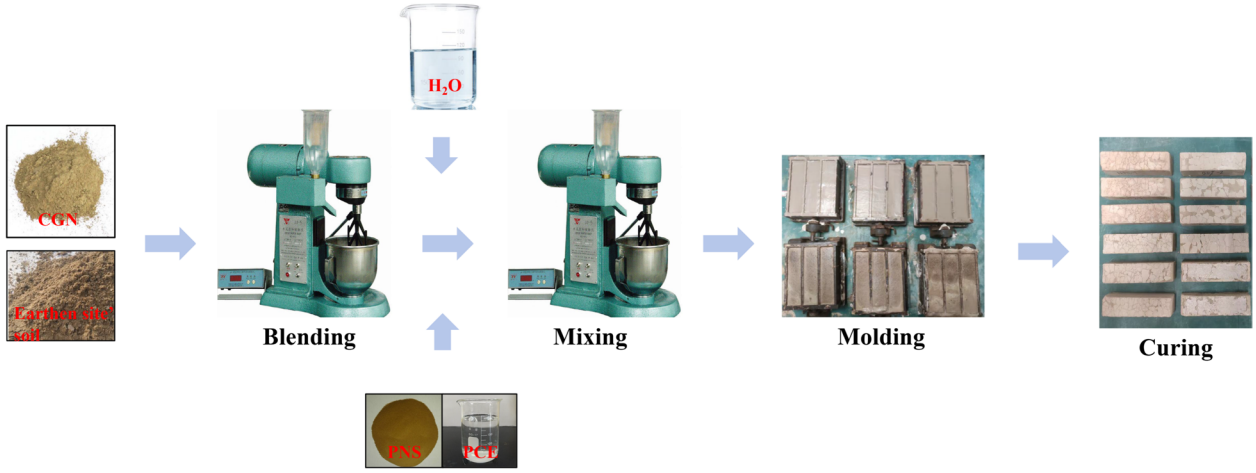

Fig. 3 Schematic illustration of producing grout

ing table in accordance with Chinese standard GB/T 17671–2021.

- After curing in air at 20 ℃ ± 2 ℃ and 50% ± 5% humidity for 3 days, the samples were demolded and further cured under the same conditions for an additional 28 days.

Testing methods

The fluidity of fresh grout was tested using a copper cone with a bottom diameter of 60 mm in accordance with Chinese standard GB/T 8077-2012. After fully mixed, fresh grout was immediately poured into the cone, and then the cone was quickly lifted. When the grout stop flowing, the average of four crossing spread diameters was recorded.

The rheological properties of fresh grout were carried out using a ZNN-D6 six-speed rotational viscometer equipped with a concentric cylinder geometry. A shearing protocol was applied that consists in a pre-shearing of 170 s^{-1} for 30 s, followed by 30 s resting period (0 s^{-1}), finial the shear rate values increased step-wise from 5 s^{-1} to 1022 s^{-1} during 210 s [34], as shown in Fig. 4. The Power-law, Bingham and Herschel-Bulkley models were applied to estimate the rheological behavior of the investigated grout, as follow:

$$\text{Power} - \text{law model}: \ \tau = K\gamma^n \tag{1}$$

$$\text{Bingham model}: \ \tau = \tau_0 + \mu\gamma \tag{2}$$

$$\text{Herschel} - \text{Bulkley mode}: \ \tau = \tau_0 + K\gamma^n \tag{3}$$

where τ is shear stress, K is consistency coefficient, n is rheological index, γ is shear rate, τ_0 is yield stress, μ is plastic viscosity. The consistency coefficient of the fresh slurry reflects the shear force, and the rheological index reflects the increasing trend of the slurry viscosity. The closer the rheological index is to 1, the slower the viscosity change [39].

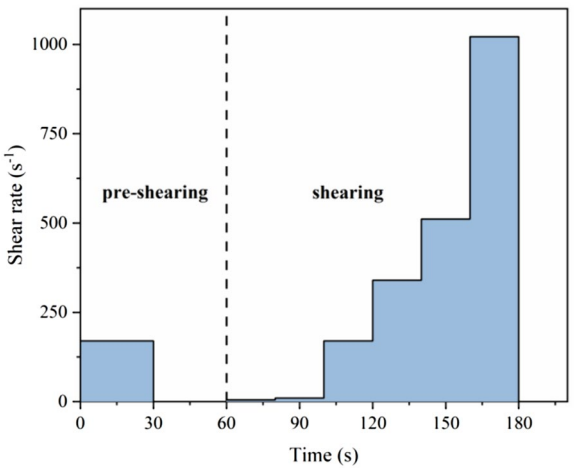

Fig. 4 Shearing protocol

The volume stability was determined using a Vernier caliper in accordance with Chinese standard GB/T 29417-2012. The Lab* color space (L, a, b) of each samples was directly measured using a Portable colorimeter (NR10QC, China), and the color difference ΔE can be calculated using the Eqs. (4):

$$\Delta E = \sqrt{(L_2 - L_1)^2 + (a_2 - a_1)^2 + (b_2 - b_1)^2} \tag{4}$$

where L represents the brightness and shade degree of the sample, ranging from 0 (black) to 100 (white), a represents the red-green degree of the sample, b represents the yellow-blue degree of the sample. L_1, a_1, b_1 are

the color coordinates of Control group, L_2, a_2, b_2 are the color coordinates of CGN based concretion with different superplasticizer.

The compressive strength and flexural strength were assessed in accordance with Chinese standard GB/T 17671-2021, utilizing a hydraulic servo universal testing machine (WDW-200, Tianshui Hongshan Testing Machine Co., Ltd., China), with a loading rate of 2 mm/min, 0.1 mm/min respectively.

The pore structure of the concretions was analyzed using an automatic mercury porosimeter (MIP, AutoPoreV9600, USA).The broken concretions were immersed in ethanol for 24 h to halt the hydration reaction, followed by drying in a drying oven at 40 °C for 48 h. Subsequently, the dried concretions were manually ground and passed through a 200-mesh standard sieve. The mineral composition of the concretions was analyzed using XRD with a scan step size of 0.02°, a scan range of 15–40°, and a scan rate of 10°/min.

Results

Fluidity, rheological properties of fresh grout

Figure 5a illustrates the fluidity of CGN-based grout with varying dosages of PCE and PNS, showing a notable increase as the dosage increases. At 2.9 wt% dosage, CGN-based grout with PCE saw a 230% increase in fluidity, stabilizing at this dosage, which is defined as critical dosage. Conversely, the fluidity of CGN-based grout with PNS continued to increase beyond 2.9 wt%. The critical dosage of PCE was found to be around 2.9 wt%, comparable to NHL2 grout (3.0 wt%) [29], but significantly higher than cement-based paste (0.5 wt%) [22].

Additionally, between 0 to 1.1 wt% dosage range, the fluidity of CGN-based grout with PNS exceeded that with PCE, contrary to observations in cement grout and lime mortars [35–37]. In cement grout, the increase in fluidity with PCE correlates with the surface coverage of the first layer of adsorbed PCE [22]. This opposite fluidity trend in CGN-based grout may be attributed to variations in the amount of PCE adsorption on the surface of blended

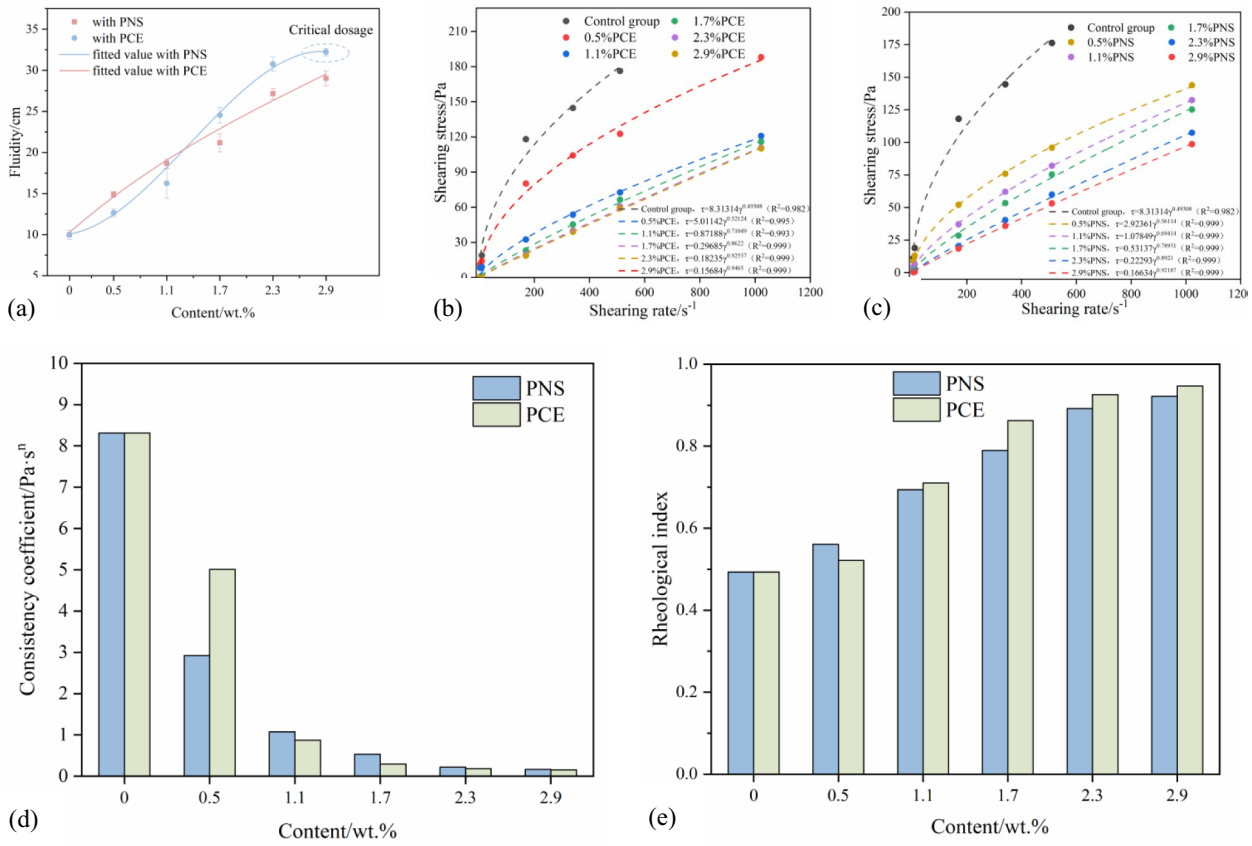

Fig. 5 **a** Fluidity of CGN based grout with PCE, PNS, **b** The shear stress-shear rate curve of CGN based grout with PCE, **c** The shear stress-shear rate curve of CGN based grout with PNS, **d** Consistency coefficient of of CGN based grout with PCE, PNS, **e** Rheological index of of CGN based grout with PCE, PNS

CGN-soil particles. Lei et al. [38] reported that up to 70% of PCE polymer is consumed by intercalating into clay (montmorillonite), while only about 30% is taken up via electrostatically induced surface adsorption. Therefore, the presence of clay in CGN-soil particles reduces PCE adsorption due to intercalation effects, resulting in lower fluidity compared to PNS. Once the clay interlayers in CGN-soil particles become saturated with PCE, its fluidity surpasses that of PNS.

Figure 5b and c depict the shear stress-shear rate curves of CGN-based grout with varying dosages of PCE and PNS. Fitting using the Power-law model, Bingham model, and Herschel-Bulkley model, the analysis reveals that the Power-law model provides higher coefficients of determination (R^2) compared to the Bingham model and Herschel-Bulkley model, effectively capturing the shear-thinning behavior of the grout. Hence, the Power-law model was employed to evaluate the rheological properties—specifically the consistency coefficient and rheological index—across all tested CGN-based grout formulations, consistent with findings in cement grout studies [34, 39], but diverging from observations in studies on self-consolidating earth concrete paste [26] and NHL grout [29].

In Fig. 5d and e, the rheological index "n" for all CGN-based grout formulations is observed to be below 1, indicating pronounced shear-thinning behavior. As the dosage of PCE and PNS increases, there is a significant decrease in the consistency coefficient alongside an increase in the rheological index. Notably, at a dosage of 0.5 wt% PCE and PNS, the consistency coefficient decreased by 39.73% and 64.83%, respectively. At higher dosages, such as 1.1 wt%, the consistency coefficient with PCE slightly trails that with PNS, correlating with earlier observations of improved fluidity due to PCE' s intercalation with clay interlayers in CGN-soil particles. This reduction in the consistency coefficient theoretically lowers the shear stress within the grout, thereby enhancing its diffusion performance [40]. The incorporation of PCE and PNS thus proves instrumental in modifying the rheological properties of CGN-based grout, underscoring their role in optimizing shear-thinning behavior and improving application performance in the repair of earthen site cracks.

Volume stability and color difference

Figure 6a illustrates the volume shrinkage of CGN-based concretion with added superplasticizer. The total volume shrinkage rate of the control group under indoor curing conditions was − 25.23%, encompassing drying shrinkage, autogenous shrinkage, and carbonation shrinkage. It is evident that the volume shrinkage rate of CGN-based grout decreases as the dosage of PCE and PNS increases, consistent with results observed in cement mortar studies [41, 42]. This indicates that incorporating PCE and PNS effectively reduces the volume shrinkage rate of CGN-based grout. For instance, the volume shrinkage rates of CGN-based grout with 2.9wt% PNS and 2.9wt% PCE were − 20.10% and − 20.54%, respectively, reflecting reductions of 6.27% and 6.86% compared to the Control group. Ge et al. [41] reported that the volume shrinkage rate of cement mortar with 0.12 wt% PCE-5C and 1.5 wt% PNS reduced by 44.44% and 7.28%, respectively. In comparison, the shrinkage reduction effect of PCE on CGN-based grout is significantly lower than that on cement mortar, and it is slightly less effective than PNS in reducing shrinkage. The reduction in shrinkage effect of PCE on cement-based materials is primarily attributed to the reduced surface tension [42]. Additionally, the adsorption amount and remaining in the aqueous phase are both related to the extent of retarding cement hydration [22], both of which influence the retardation of cement hydration. It is inferred that the chemical intercalation effect of PCE on the clay interlayer of CGN-soil particles reduces the adsorption amount, negatively impacting PCE' s

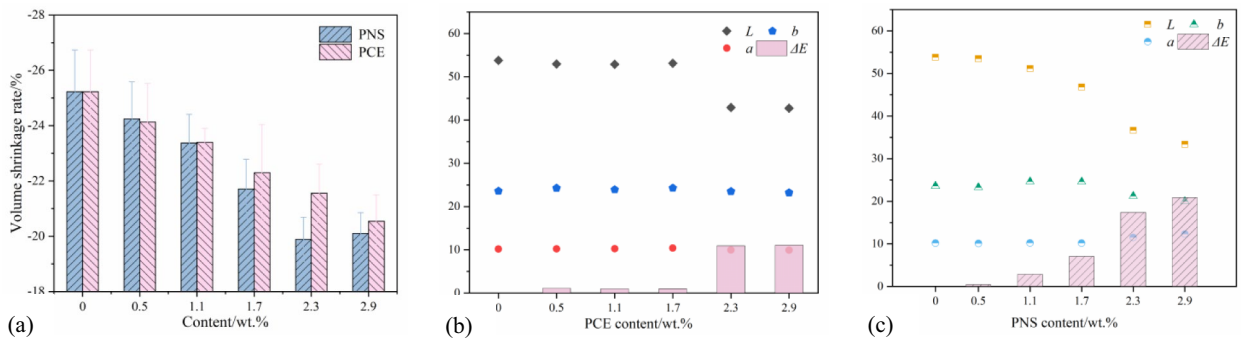

Fig. 6 **a** The volume shrinkage of CGN based grout with PCE, PNS, **b** The color difference of CGN based grout with PCE, **c** The color difference of CGN based grout with PNS

ability to reduce surface tension, thereby diminishing its shrinkage reduction effect on CGN-based grout.

The color difference of CGN-based concretion with varying additions of superplasticizer is depicted in Fig. 6b, c. With the PCE, PNS dosages increases, the brightness and shade degree (L) decreased evidently, the red-green degree (a) and yellow-blue degree (b) remain largely unchanged. It can be observed that the ΔE value gradually increases with increasing PCE, PNS dosages, which is mainly caused by the change of L value. Zhang [43] argued that ΔE value not greater than 6 is acceptable for earthen sites, which is the standard of "repairing the old as the old" widely used in cultural relics protection [44]. According to this threshold, the grout with 0.5wt% PNS, 1.1wt% PNS and 0.5wt% PCE, 1.1wt% PCE, 1.7wt% PCE can meet this standard.

Mechanical strength

Figure 7a and b illustrate the variations in compressive strength and flexural strength of CGN-based grout with different superplasticizer dosages. The trend observed with PCE dosages exhibits a "wavy shape". This contrasts with findings from CLSM studies; Wan et al. [45] noted a continuous increase in compressive strength with PCE dosages ranging from 0 to 1.0 wt% in soil comprising 8.38% clay and 75.38% silt. Conversely, Zhang et al. [46] reported a decline in compressive strength of marine dredged clay-based CLSM when PCE dosage exceeded 0.4 wt%. The disparity in CLSM performance is attributed primarily to varying clay content. Notably, CGN includes 20–30% clay [17, 47], suggesting that the complex absorption behavior of PCE on CGN and earthen site soil may explain the "wavy shape" trend observed with PCE dosages. Specifically, the compressive strength and flexural strength increased by 19.71% and 5.96%, respectively, with 0.5 wt% PCE compared to the Control group. In contrast, 1.1 wt% PCE led to a reduction of 0.94% and 8.21% in compressive and flexural strength, respectively. This indicates that 1.1 wt% PCE adversely affected the mechanical strength of CGN-based grout, suggesting an optimal PCE dosage range of 0–0.5 wt%.

PNS initially increased the compressive and flexural strength of CGN-based grout as the dosage ranged from 0 to 1.1 wt%. However, when the dosage increased from 1.1 wt% to 2.9 wt%, both strengths decreased. The maximum compressive and flexural strengths were observed at 1.1 wt% PNS, showing increases of 130.76% and 34.34%, respectively, compared to the control group. Notably, beyond 1.7 wt%, the flexural strength of PNS-treated grout fell below that of the control group, with a 1.7 wt% PNS dosage resulting in a 30.05% reduction in flexural strength. These findings align with similar results in cement-based grouts [36]. Niu et al. [48] reported that the compressive strength of cement-based paste decreased with PCE dosages above 0.12 wt% due to segregation and bleeding [35], which negatively impact the strength development of hardened grout. Thus, it is considered that 1.1 wt% is the critical dosage at which segregation and bleeding begin to affect the CGN-based grout with PNS.

XRD

The XRD patterns of CGN-based concretions are shown in Fig. 8a and b. After 28 days of curing, the main mineral compositions of the control group included quartz, clay minerals, calcite, and plagioclase, which are the primary

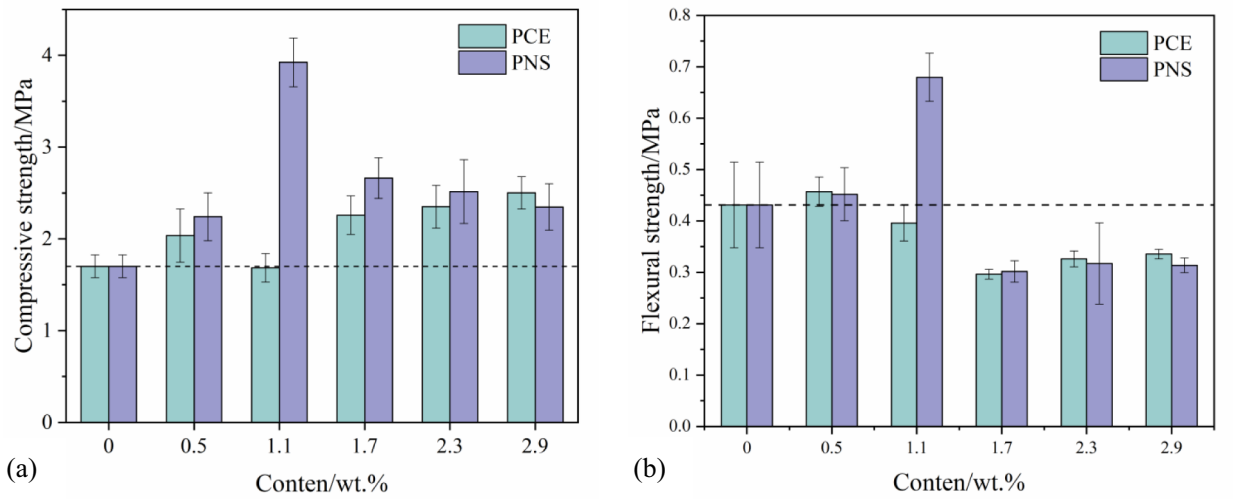

Fig. 7 **a** The compressive strength of concretion with superplasticizers, **b** The flexural strength of concretion with superplasticizers

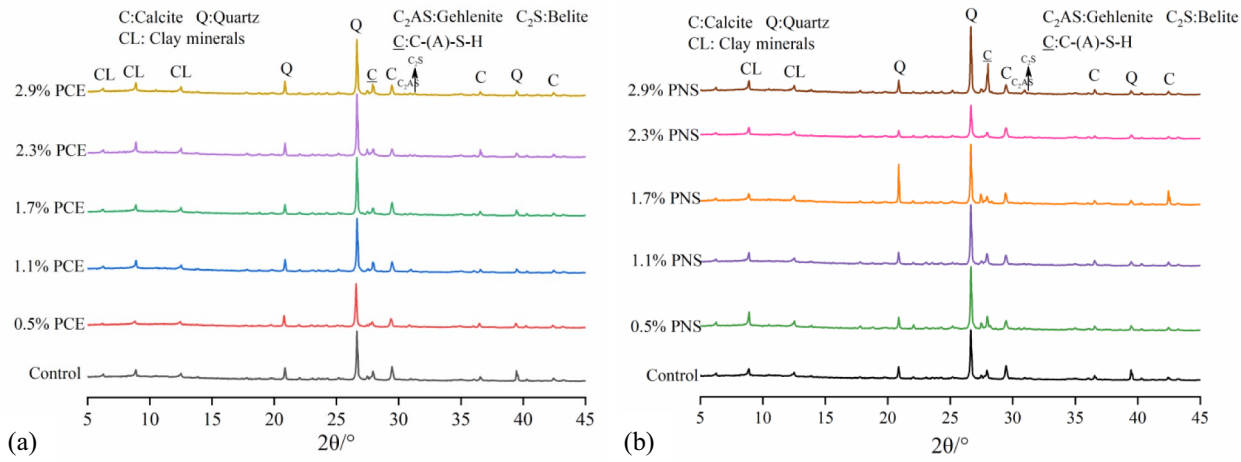

Fig. 8 **a** The XRD patterns of concretion with PCE, **b** The XRD patterns of concretion with PNS

minerals found in earthen site soil. Hydration products such as calcium silicate hydrate (C-S-H), calcium aluminate silicate hydrate (C-A-S-H), and calcite ($CaCO_3$) were generated through the reaction of CGN [18, 47]. The formation of C-S-H is primarily due to the hydration of C_2S, while C-A-S-H results from the hydration of C_2AS, as expressed in Eq. (5):

$$\begin{aligned} 2(\beta - 2CaO \cdot SiO_2) + 4H_2O \rightarrow 3CaO \cdot 2SiO_2 \cdot 3H_2O + Ca(OH)_2 \\ 2CaO \cdot Al_2O_3 \cdot SiO_2 + nH_2O \rightarrow 2CaO \cdot Al_2O_3 \cdot SiO_2 + nH_2O \end{aligned} \quad (5)$$

The intensity and FWHM of the diffraction peaks for calcium aluminate silicate hydrate (C-A-S-H) in CGN-based concretions increased slightly as the PNS dosage ranged from 0 to 1.1 wt%, then declined with further increases in PNS dosage. This trend is consistent with the observed 28-day mechanical strength. The increased hydration products filled the internal pores of the concretion, thus enhancing mechanical strength. Conversely, the intensity and FWHM of the diffraction peaks for C-A-S-H decreased with increasing PCE dosage. This finding aligns with the work of Zhang et al. [46], who reported that the adsorption of PCE molecules on the binder surface hinders the interaction between the binder and water, thereby weakening the later hydration reaction. This effect was also evident in the lower mechanical strength of the CGN-based concretion with PCE.

The presence of calcite ($CaCO_3$) indicates the occurrence of carbonation, as described in Eq. (6):

$$\begin{aligned} CaO + H_2O \rightarrow Ca(OH)_2 \\ Ca(OH)_2 + CO_2 \rightarrow CaCO_3 + H_2O \end{aligned} \quad (6)$$

Semi-quantitative analysis revealed that the calcite content in CGN-based concretions with 1.1 wt% PCE and PNS increased by 7.10% and 2.36%, respectively. This suggests that the incorporation of PCE and PNS promotes the carbonation process to some extent.

Pore structure

Figure 9a and b illustrate the pore size distribution (PSD) results for CGN-based concretions incorporating PNS and PCE. The PSD curves of the Control group shows a unimodal distribution, with the primary pore diameter around 2400 nm. Most of the concretions with added superplasticizers exhibited similar PSD characteristics to the control group, maintaining a unimodal distribution with a main pore diameter of approximately 2400 nm. However, certain samples—specifically those with 2.3wt% PCE, 2.9wt% PCE, 1.7wt% PNS, 2.3wt% PNS, and 2.9wt% PNS—displayed a bimodal pore size distribution, with an additional main pore diameter around 10000 nm. The emergence of these larger pores indicates segregation and bleeding phenomena.

The cumulative intrusion results of concretions with the addition of superplasticizer are depicted in Fig. 9c and d. By calculating the percentage of Gel pores, Capillary pores, and Stomatas for each specimen, the analysis reveals that CGN-based concretion primarily consists of capillary pores. Notably, the combined proportion of Gel pores and Capillary pores in the concretion with PCE initially decreases and then increases. For concretion with 1.1wt% PCE, the proportions of gel and capillary pores reduced by 25.76% and 13.79%, respectively. This reduction is primarily due to the combined effect of the filling of carbonation products and the dispersing capability of PCE [32]. However, increasing the PCE dosage led to a higher combined proportion of gel pores and capillary pores, attributed to the emergence of 10000 nm pores. This is caused by segregation and bleeding from excessive

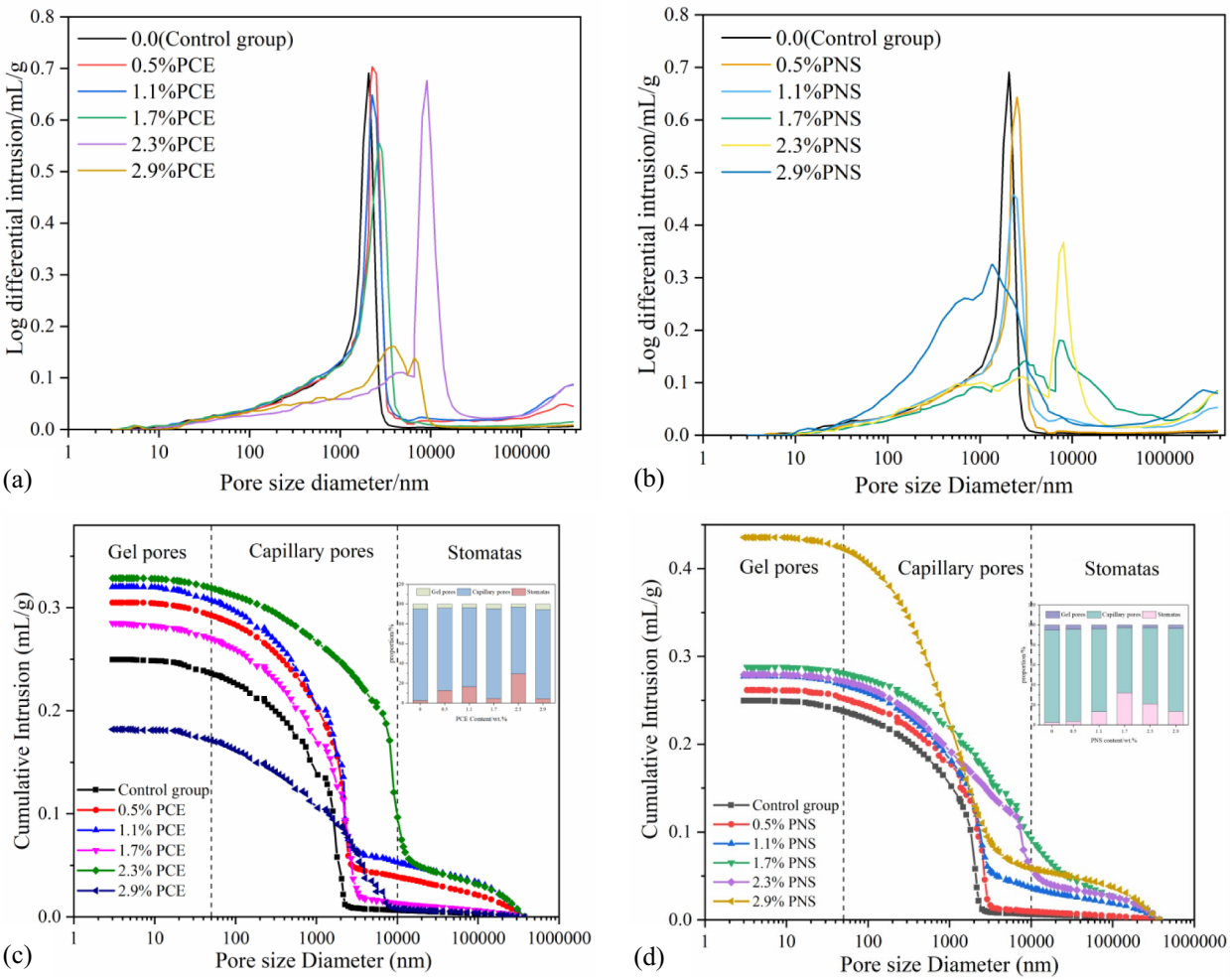

Fig. 9 **a** The pore size distribution of concretion with PCE, **b** The pore size distribution of concretion with PNS, **c** The cumulative intrusion of concretion with PCE, **d** The cumulative intrusion of concretion with PNS

superplasticizer dosage, leading to larger pores, as well as gas entrainment during mixing, which introduces bubbles [49]. Similarly, for concretion with PNS, the combined proportion of gel pores and capillary pores initially decreases and then increases. At 1.1% PNS, the proportions of gel pores and capillary pores reduced by 26.57% and 10.11%, respectively. This reduction is due to the formation of more gelatinous hydrates, including calcium silicate hydrate (C-S-H) gel and calcium aluminate silicate hydrate (C-A-S-H) gel, which envelop soil particles and form hydrate-clay aggregates that fill internal pores [18, 50]. When the PNS dosage increased to 1.7 wt%, 10000 nm pores began to appear in the CGN-based concretion, and the Stomatas proportion increased by approximately 12 times, aligning with the mechanical strength results for PNS.

Furthermore, it has been demonstrated that a low proportion of capillary pores, with more endpoints and fewer mid-sized pores, is unfavorable for paste shrinkage [41, 51]. Therefore, incorporating PCE and PNS is beneficial for reducing volume shrinkage.

Disscusion

Compatibility evaluation

A thorough compatibility evaluation is essential for selecting the appropriate type and dosage of superplasticizer for CGN-based grout. The color difference, mechanical strength, and pore structure are critical factors when assessing the compatibility between grout materials and pre-repaired materials [4, 11, 50]. Previous studies have shown that the color difference, mechanical strength, and pore structure of the Control group are similar to those of earthen sites, indicating great compatibility [12, 15]. To evaluate the compatibility of CGN-based grouts with superplasticizers, we measured quantitative properties including color difference, compressive strength, flexural

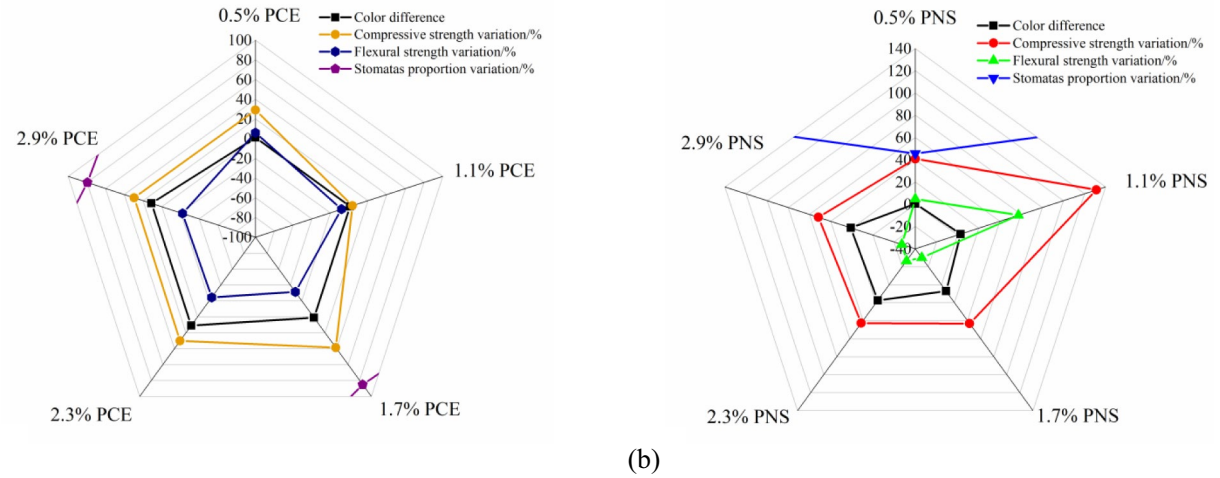

Fig. 10 Radar image of properties variations of CGN based grouts adding with PCE (**a**), PNS (**b**)

strength, and Stomatas proportion, as shown in Fig. 10, using the control group as a benchmark. The results indicated that the variation in Stomatas proportion for CGN-based grouts with superplasticizers was exceeded 80% in most cases, except for 0.5% PNS, which remained within a manageable range. This high variation of Stomatas proportion could potentially affect durability under various climate conditions. In addition, 0.5% PNS also met the color difference requirements [43].

These findings suggest that 0.5% PNS behave excellent compatible with earthen sites, but also enhance flowability and reduce shrinkage, ensuring the grout can penetrate fine cracks and voids within earthen structures and minimize the risk of new cracks forming post-repair. Additionally, this 0.5% PNS improves the rheological properties, enhancing the diffusion and injection capabilities of CGN-based grout. However, PCE showed poor compatibility with CGN-based grout, primarily due to the intercalation effect.

Numerical simulation

A 3D numerical model of a small crack was constructed using COMSOL Multiphysics to simulate the grouting process. The dimensions of this model were 60 cm × 40 cm × 5 cm, with a grouting pipe radius of 1 cm and a length of 30 cm. The burial depth was set at 20 cm (half of the crack depth), and the roughness of the crack wall was defined using a parametric surface in COMSOL Multiphysics. The model was discredited into 89095 domain units, 3256 boundary units, and 1093 edge units, as depicted in Fig. 11a. These selected dimensions of the model were sufficiently large to replicate real cracks found in earthen sites.

The material properties of the grout and earthen site soil were assumed to be homogeneous and isotropic. The grouting process was analyzed under steady-state flow conditions to simplify the analysis. Simulations with different grouting pressures (200 kPa, 100 kPa, 50 kPa, and 10 kPa) indicated that a grouting pressure of 50 kPa provided the best effectiveness. Based on real-world grouting characteristics, the lower grouting pipe nozzle was designed to maintain a constant injecting pressure boundary of 50 kPa, while the upper grouting pipe nozzle was set as a no-pressure boundary. Additionally, the six walls of the model were set as no-flow and no-slip boundaries to confine the grout within the crack. The initial pressure and velocity fields were set to zero throughout the model to represent the undisturbed state before grouting. These simulations suggest that the numerical model closely approximates real-world conditions, providing valuable insights into the grouting process.

The basic parameters of the Control group and 0.5% PNS are presented in Table 5. The apparent viscosity varies with the shear rate, and thus a least squares fitting function was utilized to model it (see Fig. 11b). This function is represented as *mu_app = m * max (gammadot, 0.01) ^ (n-1)*, where *gammadot* denotes the shear rate, m is the consistency coefficient, and n is the rheological index. The grouting process was simulated using the laminar two-phase flow physics module in COMSOL Multiphysics. The interface of the laminar two-phase flow was described using the level set method, which is formulated as follows:

$$\frac{\partial \phi}{\partial t} + u \cdot \nabla \phi = \gamma \nabla \left[\zeta IS \nabla \phi - \phi(1-\phi) \frac{\nabla \phi}{|\nabla \phi|} \right] \quad (7)$$

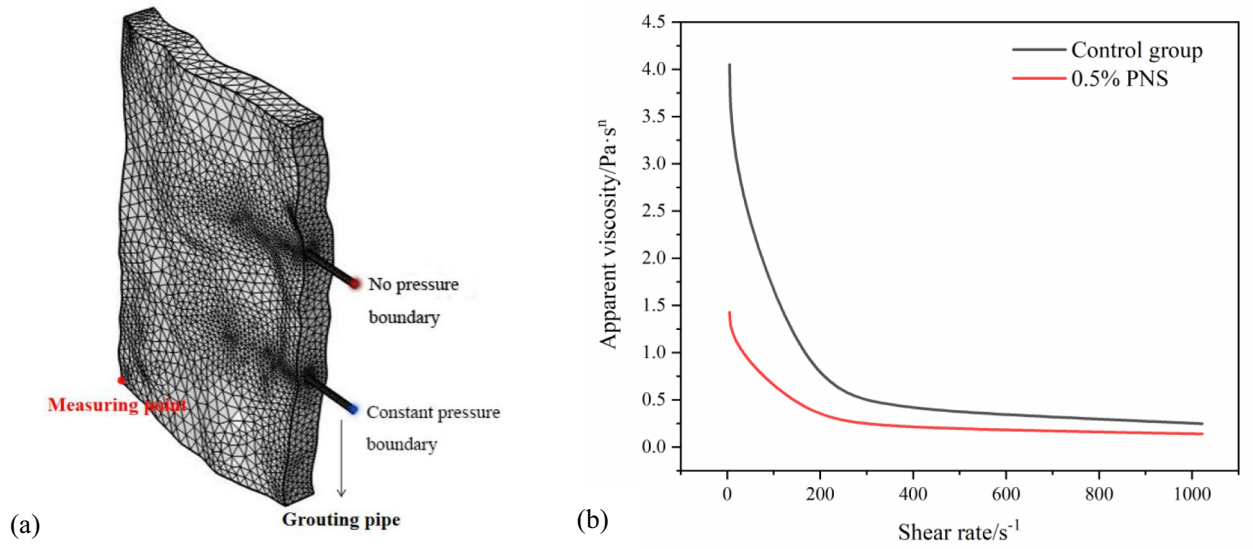

Fig. 11 **a** 3D numerical model of small crack, **b** The apparent viscosity of Control group, 0.5% PNS

Table 5 Basic parameters of Control group, 0.5% PNS

Slurry type	Consistency coefficient/Pa·s^n	Rheological index	Apparent viscosity/Pa·s^n	Grouting pressure/kPa
Control group	9.38196	0.455	mu_app1	50
0.5%PNS	2.92361	0.56114	mu_app2	50

where γ is the reinitialize parameters, ζ_{IS} is the interface thickness control parameter.

Figure 12a and b depict the slurry volume fraction of 0.5% PNS and the Control group at various time intervals. The vertical comparison shows that the slurry volume of 0.5% PNS is consistently greater at each moment, indicating its superior grouting ability compared to the Control group. Furthermore, the sectional view of the slurry volume fraction over time suggests that the diffusion pattern of the Control group primarily exhibits a "half-moon" shape. This is because the Control group slurry mainly accumulates within the total crack due to constant injecting pressure. In contrast, the 0.5% PNS slurry predominantly flows into the total crack. As a result, cracks injected by the Control group slurry are often inadequately filled, leading to some hollow areas, whereas the grouting effect of 0.5% PNS slurry is significantly enhanced.

The pressure at the measuring point, shown in Fig. 13a, consistently increases over time. Additionally, the pressure field of the 0.5% PNS is higher than that of the Control group, indicating a larger grouting volume for the 0.5% PNS slurry at the same time. The stress on the external crack wall, illustrated in Fig. 13b and c, shows that the Control group did not produce concentrated stress on the wall. In contrast, the maximum concentrated stress for the 0.5% PNS is 66.6 Pa. The concept of critical fracture pressure, proposed by Gothäll et al. [52], suggests that the initial critical fracture pressure is related to the mechanical strength, cohesion, and internal friction angle of the pre-injection soil [53]. The concentrated stress of 66.6 Pa is well below the initial critical fracture pressure of the soil of earthen sites, indicating that the 0.5% PNS does not introduce additional risks of cracking or damage to earthen sites.

In summary, the numerical simulation results suggest that the 0.5% PNS slurry exhibits a superior grouting effect without introducing additional risks of cracking.

Conclusion

In this study, we investigated the effects of Polycarboxylate superplasticizer (PCE) and Naphthalene superplasticizer (PNS) on the properties of CGN-based grout through experimental investigation, as well as simulate the grouting process of optimized CGN-based grout by COMSOL Multiphysics. Based on the findings, the following conclusions can be drawn:

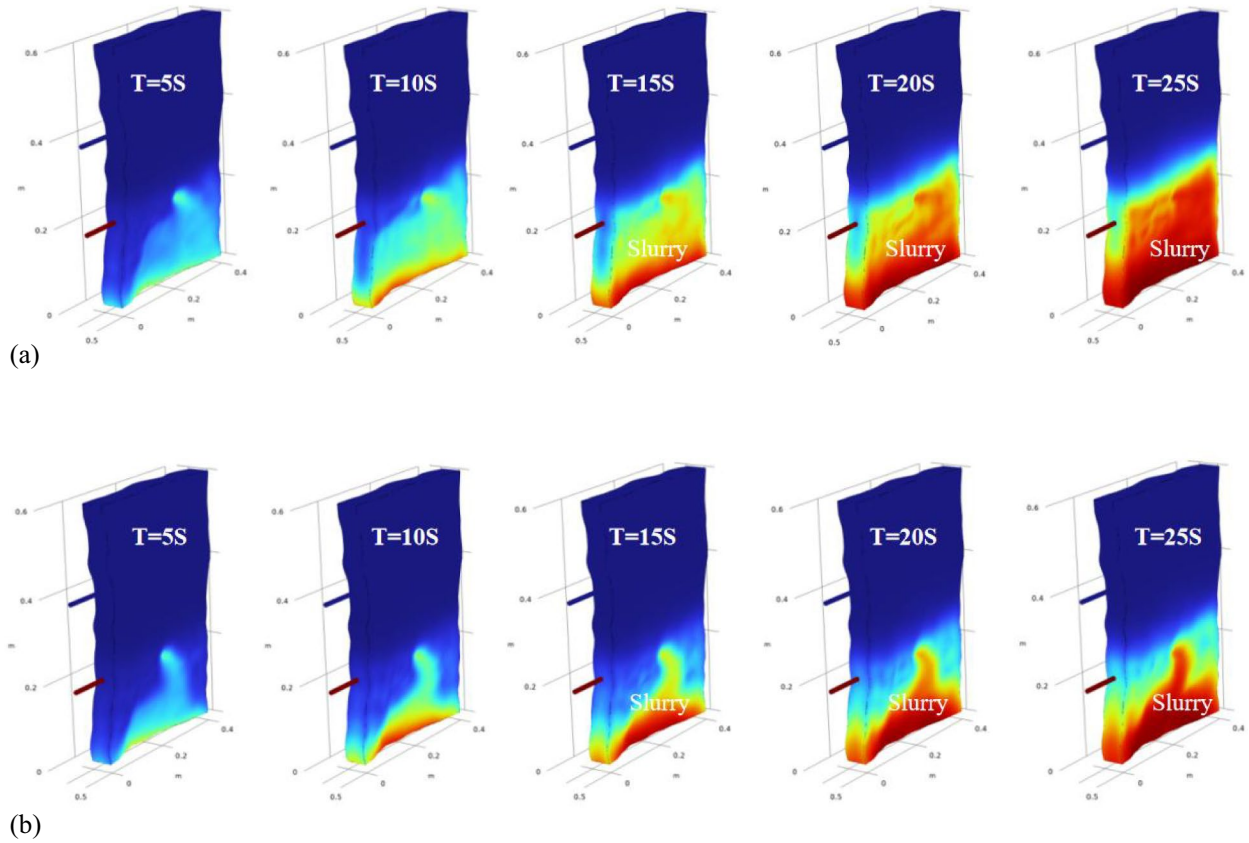

Fig. 12 **a** The slurry volume fraction figure of 0.5% PNS, **b** The slurry volume fraction figure of Control group

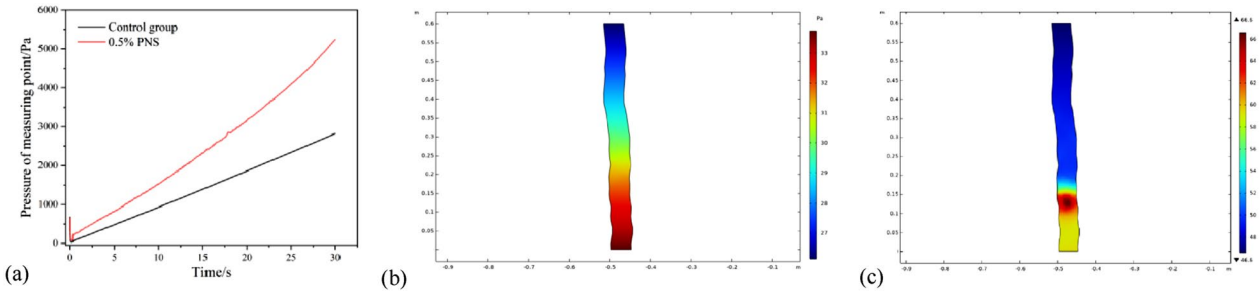

Fig. 13 **a** The pressure of measuring point, **b** The stress of inner wall of crack of the Control group, **c** The stress of inner wall of crack of the 0.5% PNS

(1) CGN based grout containing PCE, PNS is a shear-thinning fluid that conforms to the power law model. The fluidity increased and the consistency coefficient decreased with higher PCE and PNS dosage, the consistency coefficient of grout with 0.5 wt% PCE and PNS decreased by 39.73% and 64.83% respectively. The lower decrease in the consistency coefficient with PCE is due to the intercalation effect.

(2) The addition of PCE, PNS reduced the volume shrinkage rate, with 2.9wt% PCE, PNS decreasing the volume shrinkage rate by 6.86% and 6.27% respectively. The presence of PCE, PNS retarded the hydration process and lowered the proportion of capillary pores.

(3) Increasing PCE, PNS both initially increased the compressive strength and flexural strength, then decreased. 0.5wt% PCE increased the compressive strength and flexural strength by 19.71%, 5.96% respectively. 1.1wt% PNS increased the compressive strength and flexural strength by 130.76%, 34.34% than control group respectively. The excessive superplasticizer dosage leads to segregation and bleeding.

(4) PNS above 1.1wt% and PCE weakened the hydration reaction. Both PCE, PNS promote the carbonation process. The combined proportion of Gel pores and Capillary pores initially decreases, then increases with higher PCE, PNS, in which 1.1% PCE, PNS reduced the proportion of Capillary pores by 13.79%, 10.11% respectively. More carbonation products and gelatinous hydrates filled internal pores.

(5) Compatibility evaluation demonstrated that 0.5 wt% PNS behave the best compatibility with CGN-based grout, whereas PCE showed poor compatibility. Numerical simulations conducted using COMSOL Multiphysics demonstrated that 0.5% PNS provided better grouting effectiveness, larger grouting volume, and no negative impact on crack stability.

In the view of above conclusions, it can be summarized the CGN based grout with 0.5wt% PNS demonstrates excellent engineering performance and applicability. This finding is significant for addressing existing challenge of CGN based grout, offering a reliable and effective grouting materials for crack repair in earthen sites. Future studies should explore the long-term durability and environmental impact under various climatic conditions. Additionally, the potential for combining superplasticizers with other additives to further enhance grout performance warrants investigation.

Abbreviations

CGN	Calcined Ginger Nuts
PS	Polycarboxylate superplasticizer
NS	Naphthalene superplasticizer
PSD	Pore size distribution

Acknowledgements
Not applicable.

Author contributions
XW and JZ conceived and wrote this manuscript. NW and XW designed and finished the experimental ideas and experimental plans. XW completed simulation by COMSOL. NW and LZrevised and polished this manuscript. YW and WG also contributed to data analysis. All authors read and approved the final manuscript.

Funding
This work was supported by the Key Research and Development Program of Gansu Province (Project No. 23YFFA0008).

Data availability
No datasets were generated or analysed during the current study.

Declarations

Competing interests
The authors declare that they have no competing interests.

Received: 11 April 2024 Accepted: 1 August 2024
Published online: 15 August 2024

References

1. Huang KZ. The conservation of the lithic and earthy ancient buildings. Beijing: China Architecture and Building Press; 1998.
2. Shukla S. Seismic strengthening of rammed earth constructions using reinforced coatings. Braga: Universidade do Minho University; 2016.
3. Sun ML, Li ZX, Wang XD, Chen WW. Classification of deteriorations associated with many earthen heritage sites in arid areas of northwest China. Eng Geol. 2007;15(6):772–8 (**(in Chinese)**).
4. Lv J, Zhou TH, Du Q, Wu HH. Experimental investigation on properties of gypsum-quicklime-soil grout material in the reparation of earthen site cracks. Constr Build Mater. 2017;157:253–62.
5. Zhang LX, Zhang JK, Wen X, Li WH, Zhao YL. Durability assessment of calcined ginger nuts-based anchor grouts used in the conservation of earthen sites. Int J Archit Herit. 2023;17(8):1388–403.
6. Li ZX, Wang XD, Sun ML, Chen WW, Guo QL, Zhang HY. Conservation of Jiaohe ancient earthen site in China. J Rock Mech Geotech Eng. 2011;3(3):270–81.
7. Li L, Shao MS, Wang SJ, Li ZX. Preservation of earthen heritage sites on the Silk Road, northwest China from the impact of the environment. Environ Earth Sci. 2011;64:1625–39.
8. Zhang DX, Wang TR, Wang XD, Guo QL. Laboratory experimental study of infrared imaging technology detecting the conservation effect of ancient earthen sites (Jiaohe Ruins) in China. Eng Geol. 2012;125:66–73.
9. Chen WW, Liu J, Gong SY, Yang G, Wang DY, Lin GC. Researches on the durability of the SH-(C+F+CaO) slurry applied to reinforce the cracks in earthen sites. Chin J Rock Mech Eng. 2016;35(S2):4310–7 (**(in Chinese)**).
10. Xu SQ, Ma QL, Xu S. Fuzzy comprehensive evaluation of the compatibility of restoration materials—Case study in the rammed earth restoration of the M2 Han tomb in Dingtao, Shandong Province. J Cult Herit. 2022;57:131–41.
11. Peng EX, Li DD, Hu XY, Sheng Y, Chou YL, Cao W, Chen J, Li QF. Feasibility of ramming erosion area of earthen sites using solidified soil induced by an ancient curing Agent, calcined ginger nuts. Constr Build Mater. 2023;370:130442.
12. Zhang JK, Chen WW, Li ZX, Wang XD, Guo QL, Wang N. Study on workability and durability of calcined ginger nuts-based grouts used in anchoring conservation of earthen sites. J Cult Herit. 2015;16(6):831–7.
13. Chen WC, Li L, Li ZX, Zhao LY, Shao MS, Afolagboye LO. Modification of traditional Chinese ginger nut and its mechanical behavior. Constr Build Mater. 2017;144:138–46.
14. Chen WW, Zhang KW, Zhang JK, Wang DY, Zhou J, Zhang QY. Laboratory study on properties of calcined ginger nuts mixed with earthen sites' soil for grouting materials. J Cent South Univ Sci Technol. 2018;49(6):1519–25 (**(in Chinese)**).
15. Wang N, Chen WW, Zhang JK, Liao RX, Li JF, Zhao LY. Evolution of properties under realistic curing conditions of calcined ginger nut grouting mortars used in anchoring conservation of earthen sites. J Cult Herit. 2019;40:69–79.

16. Li ZX, Zhao LY, Li L, Wang JN. Research on the modification of two traditional building materials in ancient China. Herit Sci. 2013;1:1–11.
17. Shao MS, Li L, Chen WC, Liu JH. Investigation and modification of two kinds of Chinese traditional lime in cultural building relics. J Cult Herit. 2019;36:118–27.
18. Jia QQ, Chen WW, Tong YM, Guo QL. Strength, hydration, and microstructure properties of calcined ginger nut and natural hydraulic lime based pastes for earthen plaster restoration. Constr Build Mater. 2022;323:126606.
19. Qian Y, De Schutter G. Enhancing thixotropy of fresh cement pastes with nanoclay in presence of polycarboxylate ether superplasticizer (PCE). Cem Concr Res. 2018;111:15–22.
20. Baltazar LG, Henriques FMA, Jorne F. Optimisation of flow behaviour and stability of superplasticized fresh hydraulic lime grouts through design of experiments. Constr Build Mater. 2012;35:838–45.
21. Kohandelnia M, Hosseinpoor M, Yahia A, Belarbi R. A new approach for proportioning self-consolidating earth paste (SCEP) using the Taguchi method. Constr Build Mater. 2022;347:128579.
22. Zhang YR, Kong XM. Correlations of the dispersing capability of NSF and PCE types of superplasticizer and their impacts on cement hydration with the adsorption in fresh cement pastes. Cem Concr Res. 2015;69:1–9.
23. Chandra S, Björnström J. Influence of cement and superplasticizers type and dosage on the fluidity of cement mortars—Part I. Cem Concr Res. 2002;32(10):1605–11.
24. Zhang CY, Yu JW, Kong XM, Cai Y. Effect of chemical admixtures on rheological properties of mortars. J Chin Ceram Soc. 2020;48:622–31 (**(in Chinese)**).
25. Kohandelnia M, Hosseinpoor M, Yahia A, Belarbi R. Multiscale investigation of self-consolidating earthen materials using a novel concrete-equivalent mortar approach. Constr Build Mater. 2023;370:130700.
26. Kohandelnia M, Hosseinpoor M, Yahia A, Belarbi R. New insight on rheology of self-consolidating earth concrete (SCEC). Powder Technol. 2023;424:118561.
27. Baltazar LG, Henriques FMA, Jorne F, Cidade MT. Combined effect of superplasticizer, silica fume and temperature in the performance of natural hydraulic lime grouts. Constr Build Mater. 2014;50:584–97.
28. Jorne F, Henriques FMA, Baltazar LG. Influence of superplasticizer, temperature, resting time and injection pressure on hydraulic lime grout injectability. Correlation analysis between fresh grout parameters and grout injectability. J Build Eng. 2015;4:140–51.
29. Zhu JF, Hui J, Luo HJ, Zhang B, Wei XH, Wang F. Effects of polycarboxylate superplasticizer on rheological properties and early hydration of natural hydraulic lime. Cem Concr Compos. 2021;122:104052.
30. Kong XM, Li QH. Properties and microstructure of polymer modified mortar based on different acrylate latexes. J Chin Ceram Soc. 2009;37(1):107–14 (**(in Chinese)**).
31. Lu ZC, Lu JY, Liu ZW, Sun ZP, Stephan D. Influence of water to cement ratio on the compatibility of polycarboxylate superplasticizer with Portland cement. Constr Build Mater. 2022;341:127846.
32. Yan SJ, Wu YY, Lai WJ, Wang XY, Dan JM, Wang JY, Lei ZG. Effects of naphthalene superplasticizer on geopolymers activated by calcium carbide residue and Glauber's salt. Constr Build Mater. 2024;411:134599.
33. Zhou J, Wang XD, Pei QQ, Liu H, Li ZQ, Yu JJ. Effect of the pulping process on mechanical properties of slurry stones. J Lanzhou Univ Nat Sci. 2020;56(01):125–32 (**(in Chinese)**).
34. Liu QS, Lu CB, Liu B, Lu XL. Research on rheological behavior for cement grout considering temperature and hydration time effects. Chin J Rock Mech Eng. 2014;33:3730–40 (**(in Chinese)**).
35. Silva B, Pinto APF, Gomes A, Candeias A. Fresh and hardened state behaviour of aerial lime mortars with superplasticizer. Constr Build Mater. 2019;225:1127–39.
36. Zhu ZJ, Zhang QS, Zhang HS, Liu RT, Shao CZ, Ma CY, Chen MJ, Bai JW. Effect of different superplasticizers on the mechanism, workability, and microstructure of biomass-activated grouts. Constr Build Mater. 2023;373:130857.
37. Ibrahim S, Meawad A. Towards green concrete: study the role of waste glass powder on cement/superplasticizer compatibility. J Build Eng. 2022;47:103751.
38. Lei L, Palacios M, Plank J, Jeknavorian AA. Interaction between polycarboxylate superplasticizers and non-calcined clays and calcined clays: a review. Cem Concr Res. 2022;154:106717.
39. Zhu ZJ, Liu RT, Yan J, Zhang CY, Wei B. Effects of a polycarboxylate superplasticiser on the rheological properties of a Portland-sulphoaluminate cement composite slurry. Mater Lett. 2022;317:132147.
40. Shao W, Zhu ZJ, Liu RT, Wang ZH, Wei B. Effects of a polycarboxylate superplasticizer and temperature on the rheological properties of grout blended with seawater. Constr Build Mater. 2023;375:130990.
41. Ge HS, Sun ZP, Lu ZC, Yang HJ, Zhang T, He N. Influence and mechanism analysis of different types of water reducing agents on volume shrinkage of cement mortar. J Build Eng. 2024;82:108204.
42. Zhang J, Ma YF, Wang J, Gao NX, Hu ZL, Liu JP, Wang KC. A novel shrinkage-reducing polycarboxylate superplasticizer for cement-based materials: synthesis, performance and mechanisms. Constr Build Mater. 2022;321:126342.
43. Zhang JF. Discussion on color difference by chemical consolidation on earthen sites. China Cult Herit Sci Res. 2016;4:51–7 (**(in Chinese)**).
44. Wang XD, Zhang B, Pei QQ, Guo QL, Chen WW, Li FJ. Experimental studies on sacrificial layer in conservation of earthen sites. J Cult Herit. 2020;41:74–83.
45. Wan X, Ding JW, Jiao N, Zhang S, Wang JH, Guo C. Preparing controlled low strength materials (CLSM) using excavated waste soils with polycarboxylate superplasticizer. Environ Earth Sci. 2023;82(9):214.
46. Zhang S, Jiao D, Ding JW, Guo C, Gao PJ, Wei X. Utilization of waste marine dredged clay in preparing controlled low strength materials with polycarboxylate superplasticizer and ground granulated blast furnace slag. J Build Eng. 2023;76:107351.
47. Li L, Zhao L, Li Z. Study on the physical and mechanical properties of several lime materials in ancient Chinese architecture. Sci Conserv Archaeol. 2014;26(3):74–84.
48. Niu MD, Li GX, Li QQ, Zhang G. Influence of naphthalene sulphonated and polycarboxylate acid-based superplasticizer on the mechanical properties and hydration behavior of ternary binder: a comparative study. Constr Build Mater. 2021;312:125374.
49. Papayianni I, Tsohos G, Oikonomou N, Mavria P. Influence of superplasticizer type and mix design parameters on the performance of them in concrete mixtures. Cement Concrete Compos. 2005;27(2):217–22.
50. Maravelaki-Kalaitzaki P, Bakolas A, Karatasios I, Kilikoglou V. Hydraulic lime mortars for the restoration of historic masonry in Crete. Cement Concrete Res. 2005;35(8):1577–86.
51. Ge HS, Sun ZP, Yang HJ, Zheng KP, Zhang T, Cao Y. Synthesis and mechanism of shrinkage-reducing polycarboxylate superplasticizer. J Chin Ceram Soc. 2023;51(5):1293–301.
52 Gothäll R, Stille H. Fracture dilation during grouting. Tunn Undergr Space Technol. 2009;24(3):126–35.
53. Zhang LZ, Zhang QS, Liu RT, Li SC. Grouting mechanism in fractured rock considering slurry-rock stress coupling effects. Chin J Geotech Eng. 2018;40(11):2003–11.

Publisher's Note